Natural convection from a vertical surface covered with hair

J. L. Lage and A. Bejan
Department of Mechanical Engineering and Materials Science, Duke University, Durham, NC, USA

Heat transfer through a vertical skin surface covered with perpendicular hair strands of uniform density is investigated numerically. The heat transfer rate is the result of (1) direct heat transfer to the air that makes contact with the skin and (2) the heat conducted by each strand away from the skin. The hair strand and its surrounding air are not in local thermal equilibrium. Hair strands have the desirable effect of slowing the air that sweeps the vertical surface and the undesirable effect of acting as fins, thereby augmenting the overall heat transfer rate. Two distinct air flow models are considered: the Darcy model and the Forchheimer–Brinkman extended Darcy model. The overall heat transfer charts reported in this paper show that the heat transfer rate can greatly exceed the estimate based on the traditional homogeneous porous medium model. By means of numerical examples, the Darcy model is shown to be adequate for modeling air flow through mammal hair.

Keywords: hair; natural convection; insulation

Introduction

It is well known that the thermal insulation effect of hair results from trapping a layer of air next to the skin of the animal. Notorious for its low thermal conductivity, the slow-moving air blanket effectively insulates the skin against the colder environment.

Less known is the fact that the thermal conductivity of hair material is more than one order of magnitude greater than that of air. This means that in addition to slowing the air flow next to the skin, each hair strand acts as a fin that augments the heat transfer rate from the skin to the surroundings. In view of this unwanted finning effect, the existence of the hair population appears to be ruled by the trade-off between the desirable thermal insulation effect and the undesirable heat transfer augmentation effect.

This trade-off was pointed out in a short note,[1] in which conduction through hair strands was assumed to be decoupled from the air convection through the Darcy porous medium formed by hair growth. The objective of the present study is to consider a more realistic model, in which the hair strand temperature distribution is coupled to the temperature of the interstitial air flow. Another objective is to go beyond the Darcy flow model and to calculate the overall heat transfer rate when the effect of air inertia becomes important. Because of these complications, the combined conduction and natural convection phenomenon described in this article was investigated numerically.

Darcy flow

Consider the two-dimensional (2-D) vertical skin area of height H shown in Figure 1. This area is covered by a population of hair strands of uniform density n (strands/m^2). The region occupied by the hair strands can be viewed as a porous medium saturated with air, in which the hair strands constitute the solid matrix. If A_s is the cross-sectional area of one hair strand, then the porosity of this medium is

$$\phi = 1 - nA_s \tag{1}$$

In view of the different thermal conductivities of air and hair strand material, it is reasonable to expect that sufficiently close to the warm skin the hair strand is warmer than the adjacent air. In other words, it is reasonable to model the hair strand as a one-dimensional (1-D) fin surrounded by air of a different temperature. With regard to the saturated porous medium model, this assumption means that at each (x, y) position the medium is characterized by two distinct temperatures: the strand temperature $T_s(x, y)$, and the temperature of the interstitial air, $T_a(x, y)$. This two-temperature assumption distinguishes the present model from the model used in most of the current research on heat transfer through porous media,[2,3]

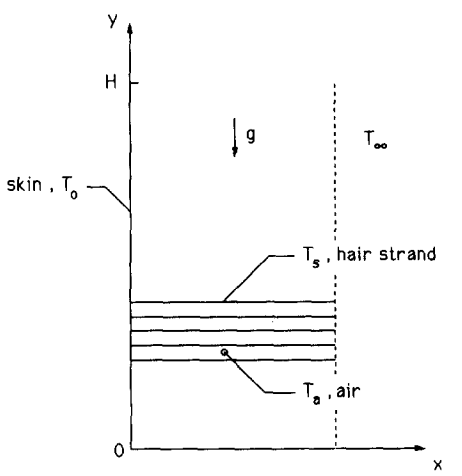

Figure 1 Two-dimensional model of hair growth on a vertical skin area

Address reprint requests to Professor Bejan at the Mechanical Engineering Department, Duke University, Durham, NC 27706, USA.

Received 31 May 1990; accepted 8 October 1990

which is based on the simplifying assumption of local thermal equilibrium.

The mass, momentum, and energy conservation equations that govern the boundary-layer flow of air through the porous matrix are

$$\frac{\partial u}{\partial x}+\frac{\partial v}{\partial y}=0 \tag{2}$$

$$\frac{\partial v}{\partial x}=\frac{Kg\beta}{v\phi}\frac{\partial T_a}{\partial x} \tag{3}$$

$$\rho c_P\left(u\frac{\partial T_a}{\partial x}+v\frac{\partial T_a}{\partial y}\right)=k_a\frac{\partial^2 T_a}{\partial x^2}+nhp(T_s-T_a) \tag{4}$$

In Equations 2–4, u and v are the local air velocity components averaged volumetrically over the space occupied only by air. The boundary-layer momentum Equation 3 is based on the assumption that the air flow is sufficiently slow that it conforms to the Darcy regime (this assumption was relaxed in the second part of this study). The porosity ϕ appears in the denominator on the right side, because v is a velocity averaged only over the air space. In other words, the product ϕv is the equivalent of the more common volume-averaged velocity used in the traditional homogeneous porous medium model.

The heat transfer coefficient h refers to the local heat transfer from the hair strand to the surrounding air, and p is the perimeter of the strand cross section. The heating effect provided by the hair structure is represented by the source term $nhp(T_s-T_a)$, which appears on the right side of the energy Equation 4. The reverse of this effect is represented by the heat-sink term $hp(T_s-T_a)$ in the equation for heat conduction along an individual hair strand:

$$k_sA_s\frac{\partial^2 T_s}{\partial x^2}-hp(T_s-T_a)=0 \tag{5}$$

The hair strand is being modeled as a 1-D fin with constant thermal conductivity (k_s), x-independent geometry (A_s, p), and constant heat transfer coefficient.

The boundary conditions that apply to the boundary-layer problem described in Equations 2–5 and Figure 1 are

$$x=0: \quad u=0 \quad T_a=T_0 \quad T_s=T_0 \tag{6}$$

$$x\to\infty: \quad v=0 \quad T_a=T_\infty \quad T_s=T_\infty \tag{7}$$

$$y=0: \quad T_a=T_\infty \tag{8}$$

Numerical method

A convenient way to nondimensionalize the governing equations and boundary conditions is to define a new set of variables that are referenced to the proper natural convection scales of the air boundary-layer flow:

$$X=\frac{x}{H\mathrm{Ra}^{-1/2}} \qquad Y=\frac{y}{H} \tag{9}$$

$$U=\frac{u}{(\alpha_a/H)\mathrm{Ra}^{1/2}} \qquad V=\frac{v}{(\alpha_a/H)\mathrm{Ra}} \tag{10}$$

$$\theta_a=\frac{T_a-T_\infty}{T_0-T_\infty} \qquad \theta_s=\frac{T_s-T_\infty}{T_0-T_\infty} \tag{11}$$

Notation

A_s	Hair strand cross-sectional area, m^2
B	Modified conductivity ratio, Equation 21
c_P	Air specific heat at constant pressure, J/kg K
C	Function, Equation 39
D	Hair strand diameter, m
Da	Darcy number, Equation 38
F	Coefficient, Equation 34
g	Gravitational acceleration, m/s^2
G	Nu departure function for the Darcy regime, Equation 32
h	Heat transfer coefficient, W/m^2 K
$\tilde{h}$	Dimensionless heat transfer coefficient Equation 20
H	Height, m
k	Thermal conductivity of homogeneous porous medium, W/m K
k_a	Thermal conductivity of air, W/m K
k_s	Thermal conductivity of hair strand, W/m K
K	Permeability of porous medium, m^2
L	Dimensionless length of numerical domain
n	Density of hair strands, strands/m^2
N_x, N_y	Numbers of nodes in the x and y directions
Nu	Overall Nusselt number, Equations 26 and 27
Nu_{CM}	Cheng–Minkowycz Nusselt number for a homogeneous medium in the Darcy regime, Equation 30
Nu_y	Local Nusselt number, Equation 29
p	Perimeter of hair strand cross section, m
Pr	Prandtl number, Equation 38
q'	Heat transfer rate per unit length, W/m
q'_a	Heat transfer rate through the skin area touched by air, W/m
q'_s	Heat transfer rate through the roots of hair strands, W/m
Ra	Darcy-modified Rayleigh number, Equation 12
T	Temperature, K
T_a	Air temperature, K
T_s	Hair strand temperature, K
T_0	Skin temperature, K
T_∞	Ambient air temperature, K
u, v	Horizontal and vertical velocity components, averaged over the air space, m/s
U, V	Dimensionless velocity components, Equations 10
x, y	Horizontal and vertical coordinates, m
X, Y	Dimensionless horizontal and vertical coordinates, Equations 9

Greek symbols

α	Thermal diffusivity of homogeneous porous medium, m^2/s
α_a	Thermal diffusivity of air, m^2/s
α_r	Relaxation factor
β	Coefficient of volumetric thermal expansion, K^{-1}
Γ	Dimensionless coefficient, Equation 38
Δ	Size of first grid spacing in the X direction
ε	Rate of grid stretching
θ_a	Dimensionless air temperature, Equation 11
θ_s	Dimensionless hair strand temperature, Equation 11
ν	Air kinematic viscosity, m^2/s
ρ	Air density, kg/m^3
ϕ	Porosity, Equation 1

$$\mathrm{Ra}=\frac{Kg\beta(T_0-T_\infty)H}{\alpha_a\nu\phi} \tag{12}$$

In Equations 9–12, α_a and Ra are the thermal diffusivity of air and the Darcy-modified Rayleigh number based on height. The problem statement, Equations 2–8, assumes the dimensionless form:

$$\frac{\partial U}{\partial X}+\frac{\partial V}{\partial Y}=0 \tag{13}$$

$$\frac{\partial V}{\partial X}=\frac{\partial \theta_a}{\partial X} \tag{14}$$

$$U\frac{\partial \theta_a}{\partial X}+V\frac{\partial \theta_a}{\partial Y}=\frac{\partial^2\theta_a}{\partial X^2}+\tilde{h}(\theta_s-\theta_a) \tag{15}$$

$$\frac{\partial^2\theta_s}{\partial X^2}-\frac{\tilde{h}}{B}(\theta_s-\theta_a)=0 \tag{16}$$

$$X=0: \qquad U=0 \qquad \theta_a=1 \qquad \theta_s=1 \tag{17}$$

$$X\to\infty: \qquad V=0 \qquad \theta_a=0 \qquad \theta_s=0 \tag{18}$$

$$Y=0: \qquad \theta_a=0 \tag{19}$$

in which $\tilde{h}$ is a dimensionless strand-air heat transfer coefficient,

$$\tilde{h}=\frac{nhpH^2}{k_a\mathrm{Ra}} \tag{20}$$

and B is a porosity-modified thermal conductivity ratio, cf. Equation 1,

$$B=\frac{k_s}{k_a}nA_s=\frac{k_s}{k_a}(1-\phi) \tag{21}$$

The number B is greater than 1, because of the large value of the conductivity ratio k_s/k_a.

The number of unknowns in this problem (U, V, θ_a, θ_s) can be reduced by 1, by integrating Equation 14 in X and invoking the boundary conditions, Equation 18. This operation yields

$$V=\theta_a \tag{22}$$

which means that V can be eliminated so that the problem reduces to solving Equations 13, 15, and 16, for U, θ_a, and θ_s. Finite-difference approximations of these equations were solved in the rectangular domain:

$$0<X<L \quad \text{and} \quad 0<Y<1 \tag{23}$$

where L is sufficiently large that the far-field conditions, Equation 18, can be satisfied. Specified on the $X=L$ boundary are the zero-flux conditions

$$\frac{\partial \theta_a}{\partial X}=0 \qquad \frac{\partial \theta_s}{\partial X}=0 \tag{24}$$

The width L was then increased to the point that the values of both θ_a and θ_s at $X=L$ dropped below 10^{-6}, as required by the actual boundary conditions, Equation 18.

The domain was covered with an orthogonal grid uniform in the vertical direction and nonuniform in the horizontal direction. The node-to-node spacing in the horizontal direction varied according to the power rule, $X_{i+1}=X_i+\varepsilon^i\Delta$, where Δ is the size of the first step (near $X=0$) and ε is the rate of grid stretching. Representative values of Δ and ε, and their effect on numerical accuracy, are presented in Table 1.

The strong coupling between Equations 13, 15, and 16 required the use of an iterative scheme. The numerical algorithm consisted of executing the following steps:

(1) solve Equation 15 for θ_a by advancing in Y;
(2) update the U value by using Equation 13;
(3) solve Equation 16 for θ_s as a function of X; and
(4) go back to step 1 using the new values of θ_a, U, and θ_s, and repeat the sequence until convergence is achieved. The convergence criterion is discussed later in connection with Equation 29.

Table 1 Effect of grid size on overall Nusselt number ($\tilde{h}=10$, $B=100$, $\phi=0.9$, $L=100$)

N_x	N_y	Δ	ε	α_r	$\mathrm{Nu}/\mathrm{Ra}^{1/2}$	*CPU*(s)
20	101	0.2	1.3029	0.80	8.3396	113
40	201	0.1	1.13405	0.75	8.4199	248
80	401	0.05	1.06331	0.65	8.4415	673

Solving Equations 15 and 13 required special care in view of the nonlinear terms of Equation 15 and the strong coupling between the two. For example, the derivative $\partial\theta_a/\partial X$ on the left side of Equation 15 was approximated by central differences, ensuring in this way a truncation error on the order of $(\Delta X)^2$ for the entire equation, where ΔX is the local grid size. In order to damp out the instabilities that may arise from the nonlinear terms, the U solution provided by Equation 13 was relaxed according to the rule:

$$U_{\text{new}}=\alpha_r U_{\text{actual}}+(1-\alpha_r)U_{\text{old}} \tag{25}$$

The relaxation factor α_r varied from 0.65 to 0.85: Several values were used to produce the solutions compared in Table 1. The finite-difference versions of Equations 15 and 16 were solved using the Tri-Diagonal-Matrix algorithm.

The effect of the grid on the accuracy and cost of the numerical solution is illustrated in Table 1. The solution in this case is represented by the overall Nusselt number,

$$\mathrm{Nu}=\frac{q_a'+q_s'}{k_a(T_0-T_\infty)} \tag{26}$$

in which the sum $(q_a'+q_s')$ is the total heat transfer rate through the area of height H per unit length in the direction normal to the plane of Figure 1 (for more on the total heat transfer rate, see the end of the Conclusions). The heat transfer contributions q_a' and q_s' result from the bare portions of the skin (the area in contact with air) and the "finned" portions (the area occupied by the roots of the hair strands), respectively. Thus

$$q_a'=\int_0^H -k_a\left(\frac{\partial T_a}{\partial x}\right)_{x=0}\phi\,dy$$

and

$$q_s'=\int_0^H -k_s\left(\frac{\partial T_s}{\partial x}\right)_{x=0}(1-\phi)\,dy \tag{27}$$

From Equations 9 and 11, it is easy to show that the overall Nusselt number is given by the integral:

$$\mathrm{Nu}=\mathrm{Ra}^{1/2}\int_0^1\left(-\phi\frac{\partial\theta_a}{\partial X}-B\frac{\partial\theta_s}{\partial X}\right)_{X=0}dY \tag{28}$$

Accuracy tests of the kind shown in Table 1 were performed. The number of nodes in the X and Y directions are listed under N_x and N_y. The second line of Table 1 shows the grid that was chosen for the $\tilde{h}=10$ solutions reported in this article. The computations were made on a MICROVAX I computer.

The dimensionless heat transfer coefficient $\tilde{h}$ has a strong effect on the horizontal extent and fineness of the grid. According to Equation 20, smaller $\tilde{h}$ values are associated with higher Rayleigh numbers, i.e., with thinner boundary layers. Consequently, it was necessary to employ a finer grid and a larger L at lower values of $\tilde{h}$. These choices are summarized in Table 2.

Table 2 Effect of group $\tilde{h}$ on grid fineness and other parameters of the numerical method

$\tilde{h}$	N_x	N_y	Δ	ε	L
0.1	80	401	0.05	1.0749	200
1	40	201	0.15	1.13405	150
10	See Table 1				

The convergence of the solution was monitored by means of the local Nusselt number,

$$\mathrm{Nu}_y = \mathrm{Ra}^{1/2}\left(-\phi\frac{\partial\theta_a}{\partial X} - B\frac{\partial\theta_s}{\partial X}\right)_{X=0} \tag{29}$$

which was calculated at each iteration (fixed Y). The solution was considered converged when the relative change in Nu_y became less than 10^{-4} percent.

Results

Sample calculations of the local Nusselt number are illustrated in Figure 2. Each curve shows that Nu_y varies approximately as $y^{-1/2}$ in the vertical direction. This trend agrees with the behavior of the local Nusselt number along an isothermal wall in contact with a homogeneous porous medium.[4]

The temperature distributions across the air bounary layer (θ_a) and along the hair strands (θ_s) are shown in Figure 3. When the heat transfer coefficient between the hair strand and the surrounding air is small ($\tilde{h}=0.1$; Figure 3, top), the air boundary layer is considerably thinner than the distance of conduction penetration along the hair strands (compare the left and right sides of Figure 3, top). Furthermore, the temperature distribution along the hair strands is almost independent of altitude. The last feature is explained by the fact that, when the air boundary layer is thin, each hair strand is bathed over most of its length by air of temperature close to T_∞ (constant).

Figure 3, bottom, shows that when the heat transfer coefficient group $\tilde{h}$ increases to 10, the air and hair strand temperature distributions are nearly the same. The hair strand temperature θ_s continues to be locally greater than the air temperature θ_a, but the local difference $\theta_s-\theta_a$ is small compared with either θ_s or θ_a. Note further that, when $\tilde{h}$ is large, the distance of conduction penetration along the hair strand decreases to match the thickness of the air boundary layer.

The local and overall Nusselt numbers defined in Equations 28 and 29 are functions of four parameters: Ra, B, $\tilde{h}$, and ϕ. Among these, only the effect of the Rayleigh number is analytically obvious, as both Nu_y and Nu are proportional to $\mathrm{Ra}^{1/2}$. The effects of B, $\tilde{h}$, and ϕ had to be investigated numerically.

The Nu results reviewed in this section acquire more meaning if they are compared with a known asymptotic value of the same quantity. That point of reference is provided in this case by the solution developed by Cheng and Minkowycz[4] for the heat transfer rate from an isothermal surface to natural convection Darcy flow:

$$\mathrm{Nu}_{CM} = \frac{q'}{k(T_0-T_\infty)} = 0.888\left[\frac{Kg\beta H(T_0-T_\infty)}{\alpha\nu}\right]^{1/2} \tag{30}$$

Recall that in the Cheng–Minkowycz model the porous medium is assumed to be homogeneous, with the effective conductivity k and thermal diffusivity α. A generalized theory of natural convection near a vertical surface embedded in porous medium has been published.[5]

The two-temperature model employed in the present study approaches the homogeneous model when $\phi\to 1$ (i.e., when $B\to 0$). In this limit, the present Nu result should approach that of Equation 30, with (k_a, α_a) replacing (k, α). In view of the present Ra definition, Equation 12, the homogeneous medium asymptote, Equation 30, can also be written as:

$$\mathrm{Nu}_{CM} = 0.888(\phi\mathrm{Ra})^{1/2} \tag{31}$$

As an alternative to documenting numerically the function $\mathrm{Nu}(\mathrm{Ra}, B, \tilde{h}, \phi)$ obtained from Equation 28, in what follows we report only the deviation of the overall Nusselt number from the Cheng–Minkowycz limit. It is easy to deduce from Equations 28 and 31 that the ratio

$$G = \frac{\mathrm{Nu}}{\mathrm{Nu}_{CM}} \tag{32}$$

is a function of only B, $\tilde{h}$, and ϕ, that is,

$$G(B,\tilde{h},\phi) = \frac{1}{0.888\phi^{1/2}}\int_0^1\left(-\phi\frac{\partial\theta_a}{\partial X} - B\frac{\partial\theta_s}{\partial X}\right)_{X=0} dY \tag{33}$$

The behavior of this function is analyzed in Figure 4. It is

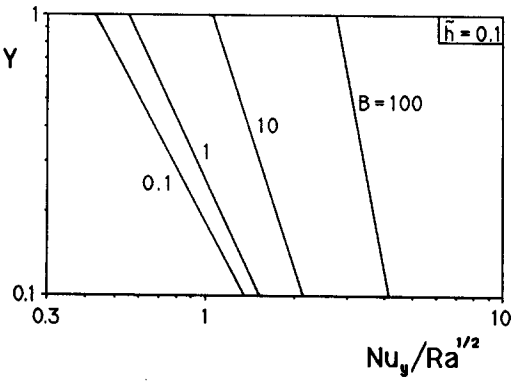

Figure 2 Local Nusselt number as a function of altitude ($\tilde{h}=0.1$, $\phi=0.9$)

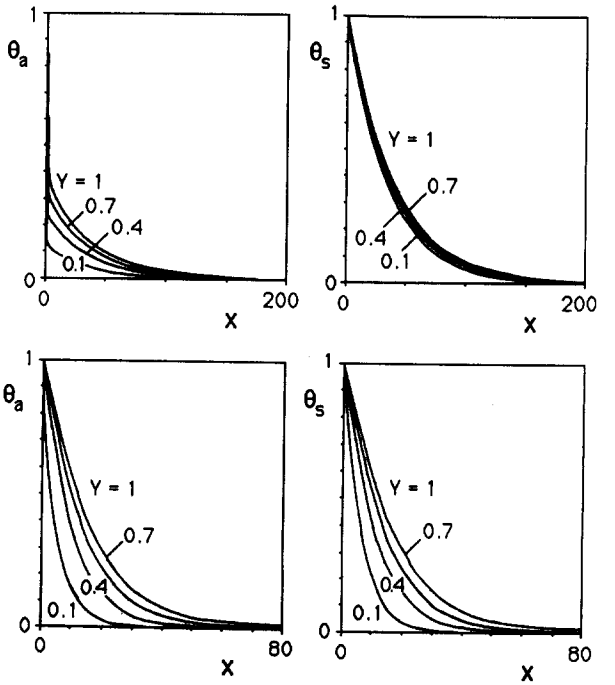

Figure 3 Distribution of temperature through the air and along hair strands. Top: $\tilde{h}=0.1$, $B=100$; bottom: $\tilde{h}=10$, $B=100$

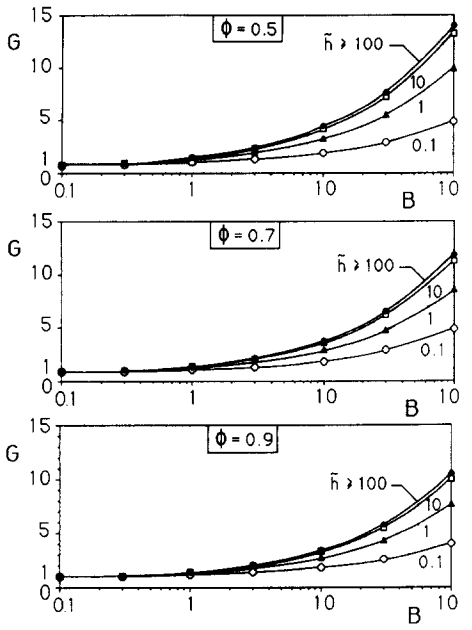

Figure 4 Departure of the overall Nusselt number from the homogeneous medium limit in Darcy flow

evident that G approaches 1 as $\phi \to 1$ and $B \to 0$, in accordance with the discussion preceding Equation 31. This agreement is an additional test of the accuracy of the present numerical calculations.

Figure 4 shows that the G ratio greatly exceeds 1 when the modified conductivity ratio B becomes greater than O(1), as in the case of hair strands surrounded by air. The G value increases monotonically with $\tilde{h}$ when $\tilde{h}$ is smaller than $O(10^2)$. When $\tilde{h}$ is greater than $O(10^2)$, it has no effect on G and the overall Nusselt number Nu. The heat transfer augmentation function of the hair strands acting as fins is confirmed by the fact that G increases with both B and $\tilde{h}$.

The porosity ϕ, which in the present model describes the heterogeneity of the porous medium, has a relatively weak effect on G. In the B range of interest, $B > 1$, lower values of ϕ (i.e., denser strands) mean higher values of G. Again, this behavior is consistent with the finning effect that can be expected from hair strands with thermal conductivity greater than that of air. In the $B < 1$ range, ϕ has the opposite effect: The effect of G drops slightly below 1 as ϕ decreases.

Forchheimer–Brinkman extended Darcy flow model

The chief message of the results presented in Figure 4 is that the overall heat transfer rate can be considerably greater than the estimate based on the homogeneous porous medium model, Equation 30. The validity of this conclusion is restricted further by the Darcy flow assumption, Equation 3. It is known, however, that when the pore Reynolds number is greater than O(10), the Darcy flow model breaks down because of the effect of fluid inertia. In addition, in high-porosity media the Darcy flow model breaks down near the wall, because the fluid feels the no-slip effect of the plane solid surface. These two effects and subsequent generalizations of the Darcy model were developed by Forchheimer[6] and Brinkman.[7]

In order to verify the validity domain of the results discussed so far, and to extend the range of this numerical study, we replaced the Darcy flow model with one that takes into account simultaneously the inertia and wall effects. These effects had been incorporated in a most general model proposed in 1981 by Vafai and Tien.[8] As shown by Kaviany and Mittal,[9] in the case of boundary-layer natural convection along a vertical wall in which the fluid has a Prandtl number of order 1 or greater, this general model recommends the following momentum equation:

$$\frac{\nu}{K}\phi v + \frac{F\phi}{K^{1/2}}(\phi v)^2 - \nu\frac{\partial^3(\phi v)}{\partial x^2} = g\beta(T_a - T_\infty) \tag{34}$$

Proceeding from left to right, the terms account for bulk viscous resistance (Darcy effect), fluid inertia (Forchheimer effect), viscous diffusion normal to the wall (Brinkman effect), and buoyancy. In the limit $K \to \infty$, Equation 34 becomes identical to the boundary-layer momentum equation in a pure fluid with $\mathrm{Pr} \gtrsim O(1)$. In the second term, F is a dimensionless factor whose selection will be discussed in connection with Equation 40.

In the new algorithm, momentum Equation 3 was replaced by Equation 34, which required the additional boundary condition for no slip at the wall, or:

$$x = 0: \quad v = 0 \tag{35}$$

Equations 34 and 35 were nondimensionalized in terms of the variables defined earlier in Equations 9–12:

$$V + \frac{\Gamma\phi}{\mathrm{Pr}}\mathrm{DaRa}V^2 - \mathrm{DaRa}\frac{\partial^2 V}{\partial X^2} = \theta_a \tag{36}$$

$$X = 0: \quad V = 0 \tag{37}$$

in which the new dimensionless groups are

$$\mathrm{Da} = \frac{K}{H^2} \qquad \mathrm{Pr} = \frac{\nu}{\alpha_a} \qquad \Gamma = \frac{F\phi}{K^{1/2}}H \tag{38}$$

The third of these parameters, Γ, is a counterpart of the inertia-term coefficient F. Note also that in the limit of low permeability, $\mathrm{Da} \to 0$. Equation 36 matches the Darcy flow momentum Equation 22.

The new algorithm consisted of solving Equations 13, 36, 15, and 16 subject to the boundary conditions Equations 17–19 and 37. It differed from the old algorithm in that the number of unknowns was four (U, V, θ_a, θ_s), instead of three (U, θ_a, θ_s). (Compare Equations 22 and 36 and note that in the present model θ_a and V are no longer identical.) The main steps in the new algorithm were

(1) solve Equation 15 for θ_a in Y;
(2) solve Equation 36 for V in X;
(3) solve Equation 13 for U in X;
(4) solve Equation 16 for θ_s in X; and
(5) go back to step 1 using the new values of U, V, and θ_s until convergence is achieved.

The discretized version of Equation 36 forms a tri-diagonal system, which was solved by a Tri-Diagonal-Matrix Algorithm. Because of the strong nonlinearity of Equation 36, the velocity components U and V had to be underrelaxed, using α_r factors from 0.3 to 0.95, depending on the particular case (ϕ, $\tilde{h}$, B, Γ, Ra, Da, Pr) that was being solved. As a general trend, cases with larger Darcy numbers required smaller relaxation factors in order to accommodate the greater role of the nonlinear term in the momentum balance.

It was necessary to perform a new set of grid fineness and numerical accuracy tests. Table 3 shows a sample of these tests for the limiting case that corresponds to the largest values of the dimensionless parameters considered in this study. The grid that was finally selected is listed in the third line. At least 12 nodes were placed between the wall and the position of maximum V in the vertical boundary layer. This feature of the

Table 3 Effect of grid size on overall Nusselt number in the extended Darcy flow model ($\tilde{h}=100$, $B=100$, $\phi=0.95$, $L=130$, $\Gamma=300$, Ra$=300$)

N_x	N_y	Δ	ε	α_r	Nu/Ra$^{1/2}$	*CPU*(s)
40	51	0.05	1.1690	0.90	8.6832	309
60	101	0.005	1.1505	0.85	8.7428	521
80	201	0.0005	1.1425	0.80	8.7691	873

Table 4 The hair thickness and density of ten mammals[11]

Mammal	D [μm]	n [strands/cm^2]	ϕ
Pika	10	11,333	0.99
Rat	12	39,000	0.99
Solenodon	14	320	0.99
Rabbit	17	20,000	0.95
Beaver	19	7,666	0.98
Lynx	27	9,000	0.95
Coyote	32	2,000	0.98
Monkey	35	1,833	0.98
Bear	50	2,500	0.95
Bison	112	450	0.97

grid was needed in order to account accurately for the effect of viscous diffusion (the Brinkman effect).

In summary, the extended Darcy flow model depends on the specification of seven dimensionless numbers, ϕ, $\tilde{h}$, B, Γ, Ra, Da, and Pr. The Prandtl number was fixed at 0.7, which is the Pr value of air. For the inertia coefficient G, we used Couland *et al.*'s[10] conclusion that

$$F\phi=\frac{C}{\phi} \tag{39}$$

in which C is a function of porosity (ϕ). A survey of the hair sizes and densities of several mammals (Table 4) shows that the porosity of mammal hair falls in the range 0.95–0.99. Therefore in the numerical work described next, ϕ was fixed at 0.95, and C was correspondingly[10] set equal to 0.1; the last of Equations 38 reduced to:

$$\Gamma=\frac{0.1}{0.95\mathrm{Da}^{1/2}} \tag{40}$$

In this way, the number of independent parameters was reduced to four, which were varied over the following ranges:

$$1<\tilde{h}<100 \qquad 30<\mathrm{Ra}<300$$

$$0.1<B<100 \qquad 0.1<\Gamma<1000 \qquad (\text{or } 1>\mathrm{Da}>10^{-8})$$

Of primary interest is the extent to which the inertia and wall effects modify the heat transfer estimate based on the simple Darcy flow model. Figure 5 shows this modification, in which the overall Nusselt number Nu is a function of the dimensionless inertia coefficient Γ. The Darcy flow estimate for Nu/Ra$^{1/2}$ is represented by the horizontal dashed line. The Nusselt number departs (falls below) this asymptote when the order of magnitude of Γ falls below 10^2 (i.e., when Da exceeds 10^{-6}). This departure becomes more pronounced as the Rayleigh number increases. However, in the entire ($\tilde{h}$, B, Ra) range presented we found that $\Gamma>O(10^2)$ in the order-of-magnitude domain in which the Darcy flow Nu estimate is adequate.

By setting Γ equal to zero in Equation 36, we found that the Nu departure from the Darcy flow asymptote results mainly from the effect of flow inertia. Comparatively, the Brinkman effect accounts for roughly 15 percent of the overall drop exhibited by Nu.

The departure from the Darcy flow limit is illustrated further in Figure 6, which shows the variation of the local Nusselt number Nu$_y$ (Equation 29). This figure confirms the observation that the Darcy flow estimate is valid when Γ is greater than $O(10^2)$.

Figure 7 shows the vertical velocity profile and the effect of extending the Darcy flow model to include the inertia and wall effects (the bottom row). The frames on the left use a logarithmic abscissa in order to emphasize the velocity distribution in the immediate vicinity of the wall. In the extended (non-Darcy) model, the velocity drops to zero as $X\to 0$: this feature is not visible on the right side of Figure 7, because of the linear scale used on the abscissa.

Another important change made visible by Figure 7 is that the vertical velocity decreases as the inertia coefficient Γ decreases. Note the drop exhibited by the maximum V value, even though $\Gamma=100$ is at the edge of the domain where the Darcy flow model is still an adequate approximation. The reduction suffered by the V maximum is considerably more severe when Γ is much smaller than 100. For example, when $\Gamma=0.1$ and the remaining parameters are the same as in the caption of Figure 7, maximum V is approximately 0.1.

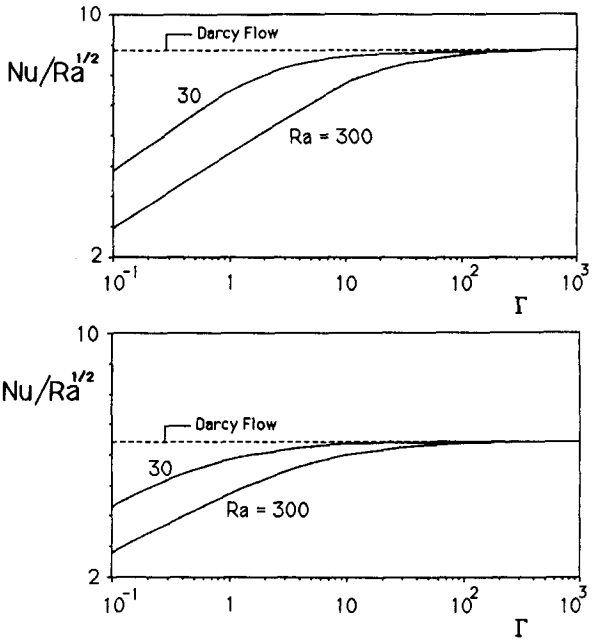

Figure 5 Departure of the overall Nusselt number from the Darcy flow limit. Top: $\tilde{h}=100$, $B=100$; $\phi=0.95$; bottom: $\tilde{h}=1$, $B=100$, $\phi=0.95$

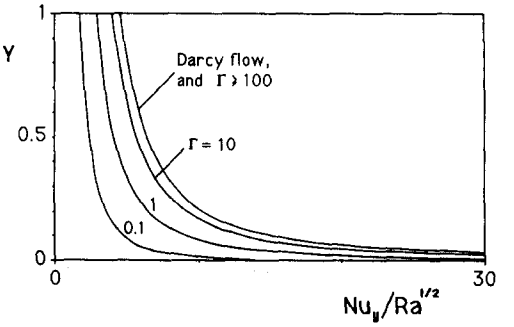

Figure 6 Departure of the local Nusselt number from the Darcy flow limit ($\tilde{h}=100$, $\phi=0.95$, Ra$=300$)

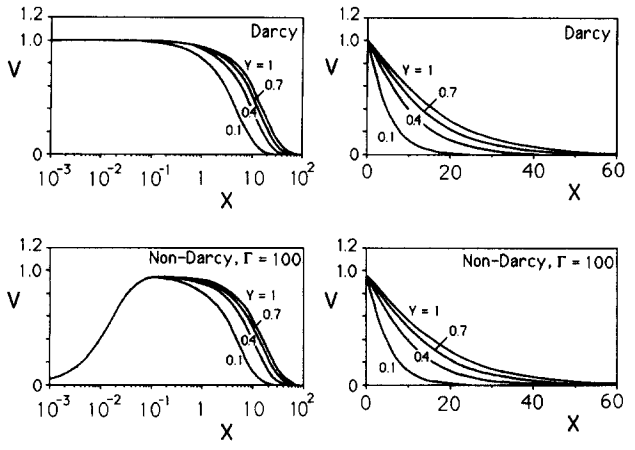

Figure 7 Departure of the vertical velocity profile from the Darcy flow limit ($\tilde{h}=100$, $B=100$, $\phi=0.95$, Ra = 300)

Conclusions

The main heat transfer results of this study are condensed in the charts of Figure 4. They show that the heat transfer rate through a vertical surface covered with hair is a function of the geometry and the physical properties of air and hair material. These results show that the heat transfer rate can greatly exceed the Cheng–Minkowycz[4] estimate based on the homogeneous porous medium model. This heat transfer augmentation effect is the result of effective heat conduction along the hair strands, and the heat transfer between each hair strand and the interstitial air.

In the preceding section, we extended the range of the overall heat transfer results by employing a flow model that accounts additionally for the effects of fluid inertia and friction against the solid surface. Another contribution of this extension was to establish the domain of validity of the Darcy flow model on which Figure 4 is based.

It is worth examining now the mammal hair data of Table 4 to see whether the Darcy flow model is adequate for natural convection heat transfer calculations. Taking as representative the hair data listed for the monkey in Table 4, we can obtain an approximate estimate for the permeability constant by invoking a model of the Kozeny type:[12,13]

$$K\sim\frac{\phi^3 D^2}{180(1-\phi)^2}=1.6\times10^{-8}\ \text{m}^2 \tag{41}$$

The order of magnitude of the height of the monkey is $H=1$ m. In this case, therefore, Equations 38 and 40 yield

$$\Gamma\sim807 \tag{42}$$

In conclusion, the Darcy flow model is adequate, because this Γ value is one order of magnitude greater than the $\Gamma\sim O(10^2)$ threshold revealed by Figure 5.

Continuing with the same numerical example, we can estimate the representative orders of magnitude of the dimensionless groups that influence the value of the overall Nusselt number Nu. By substituting $\phi=0.98$, $k_s=0.37$ W/m K, and $k_a=0.0254$ W/m K into the B definition, Equation 21, we obtain

$$B=1.17 \tag{43}$$

The Darcy-modified Rayleigh number Ra that corresponds to the K value calculated in Equation 41, can be estimated by using the properties of air and by assuming an overall temperature difference of order 40°C:

$$\text{Ra}\cong95 \tag{44}$$

Finally, for the order of magnitude of the heat transfer coefficient h, we calculate first the Reynolds number based on strand diameter and mean air velocity, $\text{Re}_D=vD/\nu$. The v scale in Darcy flow is

$$v\sim\frac{\alpha_a}{H}\text{Ra}=0.2\ \text{cm/s} \tag{45}$$

Therefore $\text{Re}_D\sim0.005$. At such low Reynolds numbers, Churchill and Bernstein's[14] correlation recommends $hD/k_a\cong0.3$; in other words,

$$h=0.3\frac{k_a}{D}=217\ \text{W/m}^2\ \text{K} \tag{46}$$

The $\tilde{h}$ defintion, Equation 20, yields finally the dimensionless value

$$\tilde{h}\sim1.8\times10^5 \tag{47}$$

The precise calculation of $\tilde{h}$ is not critical, because in the range $\tilde{h}>O(10^2)$ the $\tilde{h}$ parameter ceases to influence the value of the overall Nusselt number (see Figure 4).

In conclusion, the order of magnitude of the dimensionless groups that characterize the mammal hair are consistent with the ranges of B, Ra, and $\tilde{h}$ values used in the numerical solutions described in this study.

Another worthwhile observation is made possible by a just-published paper by Vafai and Sozen.[15] In their Figure 10, they show the parametric domain in which the assumption of local thermal equilibrium breaks down. By using (qualitatively) the present Ra range on their Figure 10 ordinate, we find that the local thermal equilibrium model would have been inappropriate for the present study. In other words, we find additional support for the two-temperature model that we adopted.

The present study and Reference 1 recounts our progress on natural convection near a surface covered with hair. The corresponding problem, in which the heat transfer mechanism is that of forced convection, were the subject of References 16 and 17. Incidentally, the analysis in the last paragraph of Reference 17 shows that the total heat transfer rate through the skin is the sum of the contributions made by the hair roots and the bare portions of the skin. That analysis is relevant to understanding the origin of Equation 26 in this article.

The most intriguing conclusion of References 1 and 16 is that there exists an optimal hair strand diameter that corresponds to a minimum heat transfer rate through the area covered with hair. Specifically, the optimum diameter D_{opt} increases with the linear size of the body covered with hair (L). When the air flow is driven by forced convection,[16] the optimum diameter increases as $L^{1/2}$, whereas in the case of natural convection,[1] D_{opt} increases as $L^{1/4}$.

These trends agree qualitatively with the measurements of mammal hair sizes. Figure 8 shows the hair diameters (D) of ten mammals,[11] with the length of the body of the animal (L) on the abscissa. The strand diameter increases with L^n, where

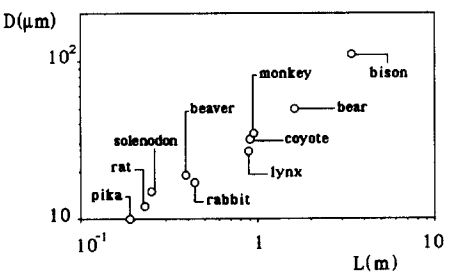

Figure 8 Actual hair strand diameters (D) and body lengths (L) of ten mammals

n is a number comparable with $\frac{1}{2}$. This trend agrees better with the theoretical result reached by assuming that forced convection is the dominant mode of heat transfer.

Acknowledgments

J. L. Lage acknowledges with gratitude the support received from Duke University and CAPES, the Brazilian Post-Graduate Education Federal Agency (Process no. 5943/87-2). A. Bejan's research was supported by Duke University.

References

1 Bejan, A. Optimum hair strand diameter for minimum free-convection heat transfer from a surface covered with hair. *Int. J. Heat Mass Transfer*, 1990, **33**, 206–209

2 Cheng, P. Geothermal heat transfer. Rohsenow, W. M., Hartnett, J. P., and Ganic, E. N. (Eds.). *Handbook of Heat Transfer Applications*, 2nd ed., McGraw-Hill, New York, 1985, ch. 11

3 Bejan, A. Convective heat transfer in porous media. Kakac, S., Shah, R. K., and Aung, W. (Eds.). *Handbook of Single-Phase Convective Heat Transfer*, John Wiley and Sons, New York, 1987, ch. 16

4 Cheng, P. and Minkowycz, W. J. Free convection about a vertical flat plate embedded in a saturated porous medium with application to heat transfer from a dike. *J. Geophys. Res.*, 1977, **82**, 2040–2044

5 Kim, S. J. and Vafai, K. Analysis of natural convection about a vertical plate embedded in a porous medium. *Int. J. Heat Mass Transfer*, 1989, **32**, 665–677

6 Forchheimer, P. Wasserbewegung durch Boden. *Z. Ver. D. Ing.*, 1901, **45**, 1782–1788

7 Brinkman, H. C. A calculation of the viscous force exerted by a flowing fluid on a dense swarm of particles. *Appl. Sci. Res.*, 1947, **1**, 27–34

8 Vafai, K. and Tien, C. L. Boundary and inertia effects on flow and heat transfer in porous media. *Int. J. Heat Mass Transfer*, 1981, **24**, 195–203

9 Kaviani, M. and Mittal, M. Natural convection heat transfer from a vertical plate to high permeability porous media: An experimental and an approximate solution. *Int. J. Heat Mass Transfer*, 1987, **30**, 967–977

10 Couland, O., Morel, P., Caltagirone, J. P. Numerical modeling of nonlinear effects in laminar flow through a porous medium. *J. Fluid Mech.*, 1988, **190**, 393–407

11 Sokolov, V. E. *Mammal Skin*, University of California Press, Berkeley, CA, 1982

12 Happel, J. Viscous flow relative to arrays of cylinders. *AIChE. J.*, 1959, **5**, 174–177

13 Eidsath, A., Carbonell, R. G., Whitaker, S., and Herman, L. R. Dispersion in pulsed systems. III—Comparison between theory and experiments for packed beds. *Chem. Eng. Sci.*, 1983, **38**, 1803–1816

14 Churchill, S. W. and Bernstein, M. A correlating equation for forced convection from gases and liquids to a circular cylinder in crossflow. *J. Heat Transfer*, 1977, **99**, 300–306

15 Vafai, K. and Sozen, M. Analysis of energy and momentum transport for fluid flow through a porous bed. *J. Heat Transfer*, 1990, **112**, 690–699

16 Bejan, A. Theory of heat transfer from a surface covered with hair. *J. Heat Transfer*, 1990, **112**, 662–667

17 Lage, J. L. and Bejan, A. Numerical study of forced convection near a surface covered with hair. *Int. J. Heat Fluid Flow*, 1990, **11**, 242–248